Molecular Crystals and Liquid Crystals

Publication details, including instructions for authors and subscription information:
http://www.tandfonline.com/loi/gmcl20

Ellipsometric Study of Liquid Crystal Infiltrated Porous Silicon

A. Marino [a b], G. Abbate [a b c], V. Tkachenko [b], I. Rea [a d], L. De Stefano [d] & M. Giocondo [c]

[a] Dipartimento di Scienze Fisiche, Università di Napoli "Federico II", Naples, Italy

[b] CNR-INFM - Coherentia c/o Physics Department, University of Naples "Federico II", Naples, Italy

[c] CNR-INFM Licryl — Liquid Crystal Laboratory c/o Physics Department, University of Calabria Rende (CS), Italy

[d] CNR Institute for Microelectronics and Microsystems (IMM), Naples, Italy

Version of record first published: 22 Sep 2010

To cite this article: A. Marino, G. Abbate, V. Tkachenko, I. Rea, L. De Stefano & M. Giocondo (2007): Ellipsometric Study of Liquid Crystal Infiltrated Porous Silicon, Molecular Crystals and Liquid Crystals, 465:1, 359-370

To link to this article: http://dx.doi.org/10.1080/15421400701206220

Mol. Cryst. Liq. Cryst., Vol. 465, pp. 359–370, 2007

ISSN: 1542-1406 print/1563-5287 online
DOI: 10.1080/15421400701206220

Ellipsometric Study of Liquid Crystal Infiltrated Porous Silicon

A. Marino
Dipartimento di Scienze Fisiche, Università di Napoli "Federico II", Naples, Italy; CNR-INFM – Coherentia c/o Physics Department, University of Naples "Federico II", Naples, Italy

G. Abbate
Dipartimento di Scienze Fisiche, Università di Napoli "Federico II", Naples Italy; CNR-INFM – Coherentia c/o Physics Department, University of Naples "Federico II", Naples, Italy; CNR-INFM Licryl – Liquid Crystal Laboratory c/o Physics Department, University of Calabria Rende (CS), Italy

V. Tkachenko
CNR-INFM - Coherentia c/o Physics Department, University of Naples "Federico II", Naples, Italy

I. Rea
Dipartimento di Scienze Fisiche, Università di Napoli "Federico II", Naples Italy; CNR Institute for Microelectronics and Microsystems (IMM), Naples, Italy

L. De Stefano
CNR Institute for Microelectronics and Microsystems (IMM), Naples, Italy

M. Giocondo
CNR-INFM Licryl – Liquid Crystal Laboratory c/o Physics Department, University of Calabria Rende (CS), Italy

Porous silicon (PS) based devices are nowadays under an intense and widespread investigation in the optoelectronic and sensing fields. Recently, the range of

We are deeply grateful to Dr. Thomas Wagner, by Lot-Oriel Europe (Germany), for technical support about the WVASE32™ software, and to Mr. Alfredo Pane, by CalcTec Srl (Italy), for technical support in the LC infiltration.

Address correspondence to A. Marino, Dipartimento di Scienze fisiche, Via Cinthia Monte S. Angelo, Naples 80126, Italy. E-mail: antigone@na.infn.it

possible applications has been widened by the use of the liquid crystals (LCs), which can be infiltrated in the PS sponge-like structure. The large changes of the optical properties, as exhibited by LCs under the action of electrical or thermal fields, allow developing a new family of optical devices like tunable PS based multilayer mirrors, microcavities and optical filters.

In this work, we have optically characterized the LC-PS heterogeneous composite as a guest-host system by means of the variable angle spectroscopic ellipsometry (VASE). A PS layer, 450 nm thick, has been infiltrated with the nematic LC 5CB, and the main optical parameters, anisotropic refractive indices and thickness of both materials, have been estimated below and above the isotropic transition temperature, at 27.0°C and 38.0°C respectively. We have found a clear indication that the LC molecules tend to align parallel to the direction of the pore columns.

Keywords: anisotropy; ellipsometry; liquid crystal; porous silicon; refractive index

INTRODUCTION

Silicon is the dominant material in the microelectronics industry but it does not play a major role in optoelectronics because its optical properties cannot be easily modulated by external applied fields.

In order to transfer the advantages of the well-established silicon processing infrastructure to the optoelectronics domain, the physical and optical properties of silicon need to be manipulated. Porous silicon is a unique material that can provide the link between the silicon technology and the optoelectronic devices because it is inherently silicon-based, which facilitates device integration into a standard microelectronics platform, and it is porous, which can allow the tuning of its optical properties [1,2]. The fabrication of tunable PS photonic bandgap devices opens the door for the next generation of optical interconnect and optical switching technology.

PS is a nanostructured material, produced by the electrochemical etch of crystalline silicon at low cost and high repeatability, which is by far used in photonic applications, for instance in the realization of passive optical components, such as filters or photodetectors, or in the optical sensing.

PS main feature, from a material point of view, is its sponge-like morphology. During the production process, by changing the time and the intensity of the etching current, it is possible to obtain layers with different thickness and porosity, which is defined as the volume fraction of air present in a layer. In this way, the dielectric properties of porous silicon, and in particular the refractive index n, can be namely modulated between those of crystalline silicon ($n = 3.54$, $porosity = 0$)

and air ($n = 1$, *porosity* $= 100\%$). Actually, the porosity can be varied between 50 and 81%. Since the etching process is self-stopping, it is possible to fabricate mono and multilayered structures such as Fabry-Perot interferometer, Bragg reflectors, optical microcavity and even aperiodic sequences, such as the Thue-Morse quasi-crystals [3].

Moreover, PS can be turned in an optically active material if a suitable electro-optic or thermo-optic species, like for instance a LC, is infiltrated into the pores. In order to improve the device design, it is a primary need to get better knowledge of the optical and morphological properties of the PS host, and the LC guest inside it. Optical characterization of PS-LC composite thin films is complicated by the anisotropic nature of both the PS layer and the infiltrated LC. Nevertheless, VASE is a suitable technique to manage such a complex anisotropic system, to carry out high precision measurements of the anisotropic refractive index, the porosity, and the thickness of heterogeneous layer. Moreover, VASE can give crucial information on the amount of the infiltrated LC and on the director orientation inside the pores.

In this work we used the 5CB nematic liquid crystal, as one of the most widely studied and commonly used for non-display device prototypes. The VASE optical characterization of the liquid crystal infiltrated porous silicon is presented here in the wavelength range between 450 and 1600 nm, and for 2 temperatures, one below and one above the clearing point.

ELLIPSOMETRY

Standard Spectroscopic Ellipsometry (SE) is based on the measurement of two physical quantities: the relative phase change, Ψ, and the relative amplitude change, Δ, suffered by incident light when reflected (or transmitted) by a layered structure. These two parameters are linked to the reflection (or transmission) coefficients, which are themselves related to the optical response of the surface: the Ψ's and Δ's spectra depend on the refractive indices of the layers, on their thickness and, in the case of anisotropic films, on the orientation of their optical axis (of course, they depend on any physical parameters that affect the optical behaviour of the material, for instance on temperature).

Ellipsometry application to anisotropic media (Generalised Ellipsometry) requires the adoption of the 2×2 Jones matrix formalism. In this way it is possible to generalise the Ψ and Δ parameters to the case when a change occurs in the light polarisation. The six GE parameters

are linked to the Jones matrices of reflected ($\mathbf{J^r}$) or transmitted ($\mathbf{J^t}$) beam through the following equations:

$$\begin{aligned} \tan\Psi \cdot e^{i\Delta} &= \frac{J_{pp}}{J_{ss}} \\ \tan\Psi_{sp} \cdot e^{i\Delta_{sp}} &= \frac{J_{sp}}{J_{ss}} \\ \tan\Psi_{ps} \cdot e^{i\Delta_{ps}} &= \frac{J_{ps}}{J_{pp}} \end{aligned} \tag{1}$$

where $\mathbf{J} = \mathbf{J^r}$, $\mathbf{J^t}$ and $\mathbf{J^r} = \begin{pmatrix} r_{pp} & r_{sp} \\ r_{ps} & r_{ss} \end{pmatrix}$, $\mathbf{J^t} = \begin{pmatrix} t_{pp} & t_{sp} \\ t_{ps} & t_{ss} \end{pmatrix}$ with r_{pp}, r_{ss}, r_{ps}, r_{sp} (t_{pp}, t_{ss}, t_{ps}, t_{sp}) representing the reflection (transmission) coefficients for *p*-, *s*-, and cross-polarisations, respectively.

However, the Jones matrix formalism is based on the assumption of a completely polarised light. When a significant amount of reflected or transmitted light becomes depolarised, as it is generally the case with LC, it may be necessary to introduce the Mueller Matrix (MM) representation. In this scheme, a 4×4 matrix connects the Stokes vectors representing the input and the output beam, as described in Eq. (2):

$$\begin{bmatrix} S_0 \\ S_1 \\ S_2 \\ S_3 \end{bmatrix}_{OUT} = \begin{bmatrix} M_{11} & M_{12} & M_{13} & M_{14} \\ M_{21} & M_{22} & M_{23} & M_{24} \\ M_{31} & M_{32} & M_{33} & M_{34} \\ M_{41} & M_{42} & M_{43} & M_{44} \end{bmatrix} \cdot \begin{bmatrix} S_0 \\ S_1 \\ S_2 \\ S_3 \end{bmatrix}_{IN} \tag{2}$$

In our measurements, we used a Variable Angle Spectroscopic Ellipsometer (VASE®) from J. A. Woollam Company [4]. This instrument is equipped with a rotating analyser that incorporates an adjustable compensator before the sample. Through it all four Stokes parameters can be produced for the input beam; instead, due to the absence of a retarder after the sample, only the first three parameters of the output beam can be measured. Thus, our instrument provides access to the first three rows of MM elements, each one normalized to the M_{11} element. In case of anisotropic, depolarising media, with non-zero off-diagonal elements, our eleven elements can give a complete description of the optical properties of the sample [5,6].

In order to get a large amount of data, the GE as well as the MME parameters were measured as a function of both angle of incidence and wavelength, in the spectral range from 450 to 1600 nm.

All data were simultaneously analysed using WVASE32™ software to determine the sample refractive index, thickness, silicon porosity and the amount of LC inside the pores. Samples were mounted on a processor-controlled hot-stage which allowed us temperature stability and accuracy of 0.1°C.

EXPERIMENTAL DETAILS

PS layers were prepared by electrochemical etching of a highly doped p^+-silicon wafers, $\langle 100 \rangle$ oriented, 0.01 Ωcm resistivity, and 400 μm thick. Samples were fabricated in dark light at room temperature using a solution of 30% volumetric fraction of aqueous hydrofluoric acid (HF, 50% wt) and 70% of Ethanol. The overall dissolution reaction of silicon inside hydrofluoric acid can be expressed by this equation,

$$\mathrm{Si(s)} + 6\mathrm{F}^- + 2\mathrm{H}^+ + 2\mathrm{h}^+ \rightarrow \mathrm{SiF}_6^{2-} + \mathrm{H}_2\mathrm{(gas)}.$$

Before anodization, we removed the thin film of native oxide from the silicon wafer by rapid rinsing it in a diluted HF solution.

LC was infiltrated in the PS sample under vacuum conditions in a low vacuum chamber in order to obtain a uniform distribution of liquid crystals throughout the porous silicon matrix: the absence of air in the pores allows the liquid crystal to be efficiently infiltrated into the microcavity. Furthermore, the LC was heated above the clearing point, so that to facilitate the infiltration process due to the lower LC viscosity in the isotropic phase.

The optical characterization of the PS film was done before and after infiltration with 5CB, in the whole spectral range and at the 2 temperatures of 27.0°C and 38.0°C. Various porous silicon monolayer samples of about 80% porosity and thickness from 150 nm up to 450 nm were realized. Ellipsometric data were acquired at different incidence angles, varying from 60° to 70°. Here we discuss the results for a 450 nm sample, at an incidence angle of 60°.

In Figure 1, we report the SEM images of a top view and a cross section of a thicker sample of PS monolayer as an example of the spongy structure.

Due to inherent inhomogeneity at mesoscale in the layer plane of porous silicon, previous SE characterizations of this material were performed successfully only adopting the Bruggeman Effective Medium Approximation (EMA) [7], also including a sequence of sublayers in order to take into account the inhomogeneity along the layer normal [8]. We have further refined the latter model adopting a graded model instead of a stack of EMA sub-layers.

The graded model allows for a set of N linear variations of the physical parameters between $N + 1$ nodes distributed along the thickness. The latter model has proven to be more effective than the formers, especially when considering the non-uniform distribution along the stratification direction of the infiltrated liquid, in addition to the morphological one of the pores.

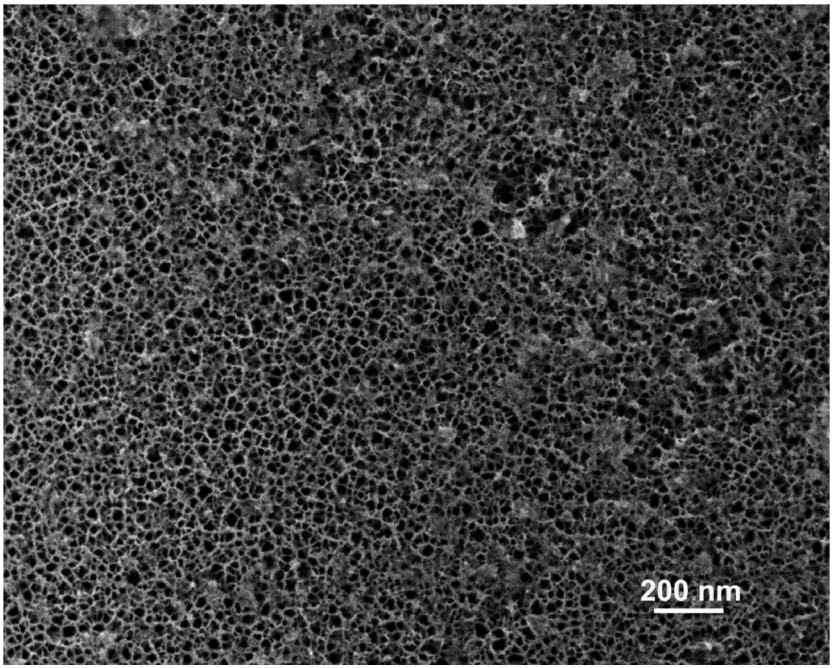

FIGURE 1 Top view SEM images of $p^+(100)$ silicon sample etched with aqueous HF. The mesopores have an average pore diameter of $\sim 10 \div 50$ nm.

The Mean Squared Error (MSE) value, which is a measure of the difference between experimental and model data, is the indicator of the goodness of the employed model, as usual in SE measurements. An increase of the complexity of the model can be justified if it is physically sound and leads to a decrease of MSE by one order of magnitude (or more). In our case, both conditions are completely fulfilled.

In the case of inhomogeneous materials at mesoscale, the EMA layer provides a method to mix 2 or 3 sets of optical constants together: for PS samples, a mix of void ($\sim$80%) and Si ($\sim$20%) was considered; for 5CB + PS samples, void ($\sim$ 30%), 5CB ($\sim$50%) and Si ($\sim$20%) were the 3 components.

In our model, the graded layer was divided by three nodes (see Figure 2): one at the bulk silicon-PS interface (Node 1); one in an intermediate position inside the PS (Node 2); the third at the PS-air interface (Node 3). Measurements on the empty sample provided the PS thickness to be 478 nm, the position of Node 2 at $\sim$42% of the thickness, and the silicon fraction for each node. These values were kept fixed for the infiltrated samples.

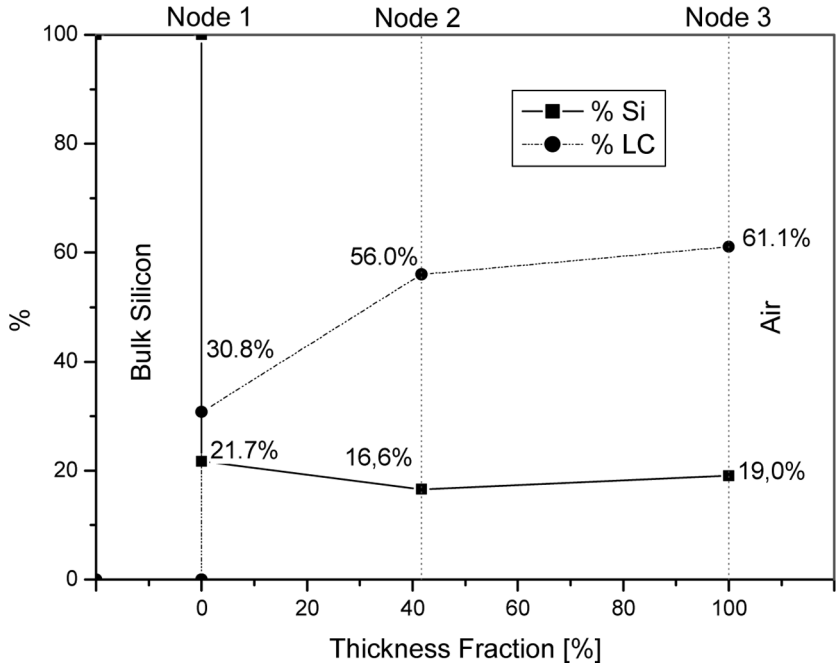

FIGURE 2 Schematic of the used graded-EMA model for the infiltrated porous silicon sample. The best fitted values for the material composition percentage are shown.

For the empty PS sample, acquired data together with fitted results are shown in Figure 3a. For an infiltrated sample, the same model was implemented by fixing the Si fraction and introducing the third material, which is a LC fraction inside EMA layer. Measured data and fitted results at 27.0°C, i.e., in the nematic phase, are shown in Figure 3b, and at 38.0°C, i.e., in the isotropic phase, in Figure 3c.

Comparison of Ψ data for empty PS and filled one confirms the high sensitivity of the spectroscopic ellipsometry to the volume fraction change, by addition of LC material.

The substitution of the air inside the pores by the LC increases the average refractive index of the layer resulting in a red shift of the Ψ parameter. The shift slightly increases also with the temperature (see Fig. 4) due to the LC effective index rise.

Ordinary, extraordinary refractive indices, and the birefringence as a function of λ and depth can be immediately calculated from the fitted data resulting from the described model. Effective n_o, n_e, and

$\Delta n = n_e - n_o$ values for the whole samples, obtained by the simple following formula,

$$n_{o,e} = \frac{1}{d}\int_0^d n_{o,e}(z)dz$$

are shown in Figure 5. Figures 5a and 5b show a general and obvious increase in the refractive indices by substituting the air in the pores with LC material. Moreover, one can observe an increase in n_o and

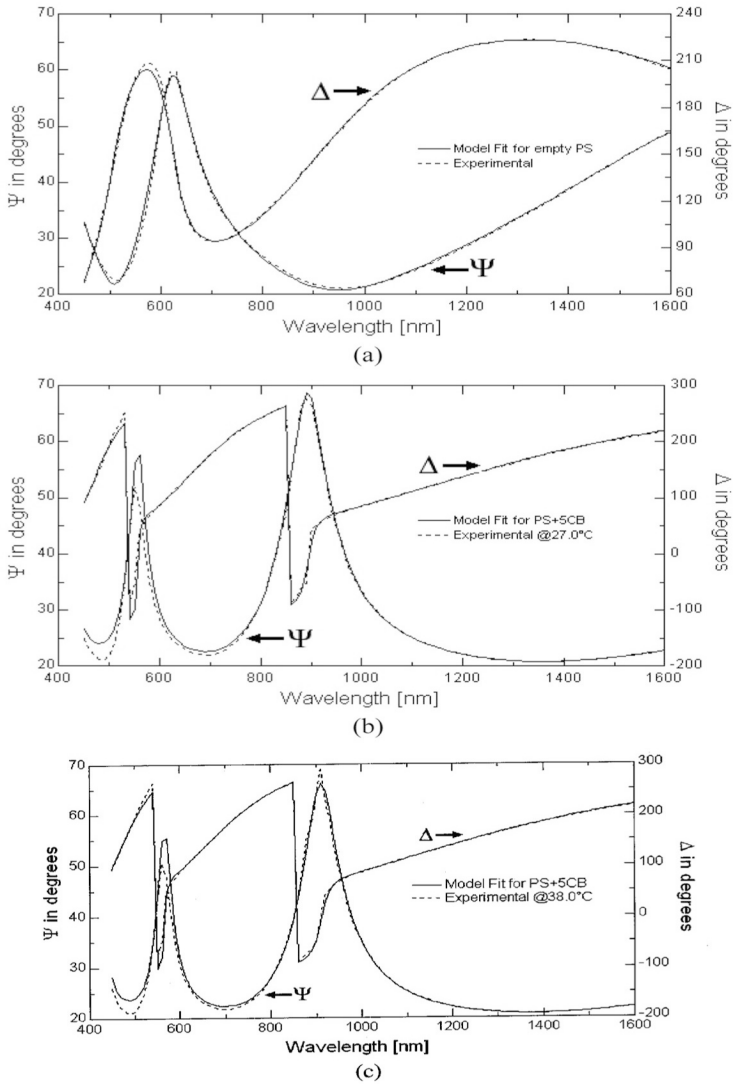

FIGURE 3 Experimental (dashed curve) and calculated (solid curve) $\Delta(\lambda)$ and $\Psi(\lambda)$ ellipsometric spectra for J_{pp}/J_{ss} ratio: (a) porous silicon without any infiltration, (b) 5CB infiltrated PS in the nematic phase, (c) 5CB infiltrated PS in the isotropic phase.

decrease in n_e with the nematic-isotropic transition of LC. This is a clear first indication of the major role played by the infiltrated LC in the sample optical behaviour. The behaviour of the birefringence, shown in Figure 5c, allows us to better figure out what physically may happen. In general, birefringence decreases when inserting a isotropic dielectric into the pores [9], because the optical contrast decreases. The results in

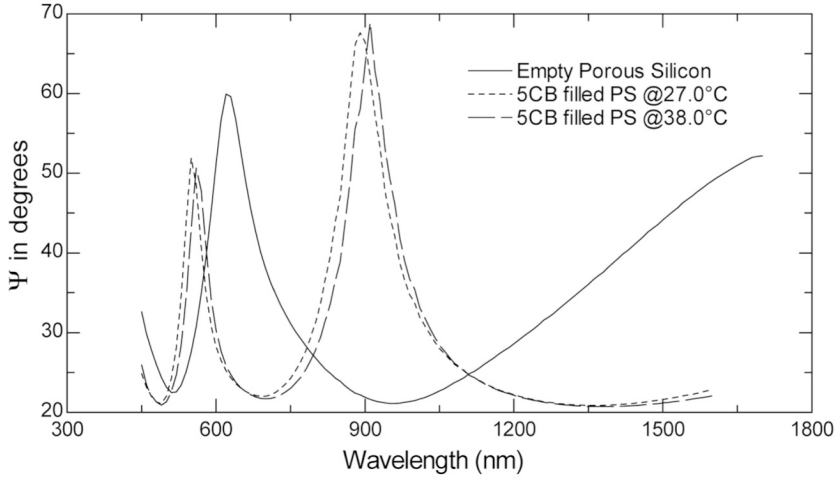

FIGURE 4 Comparison between the Ψ spectra for the empty porous silicon sample, the infiltrated sample at 27.0°C, and the infiltrated sample at 38.0°C.

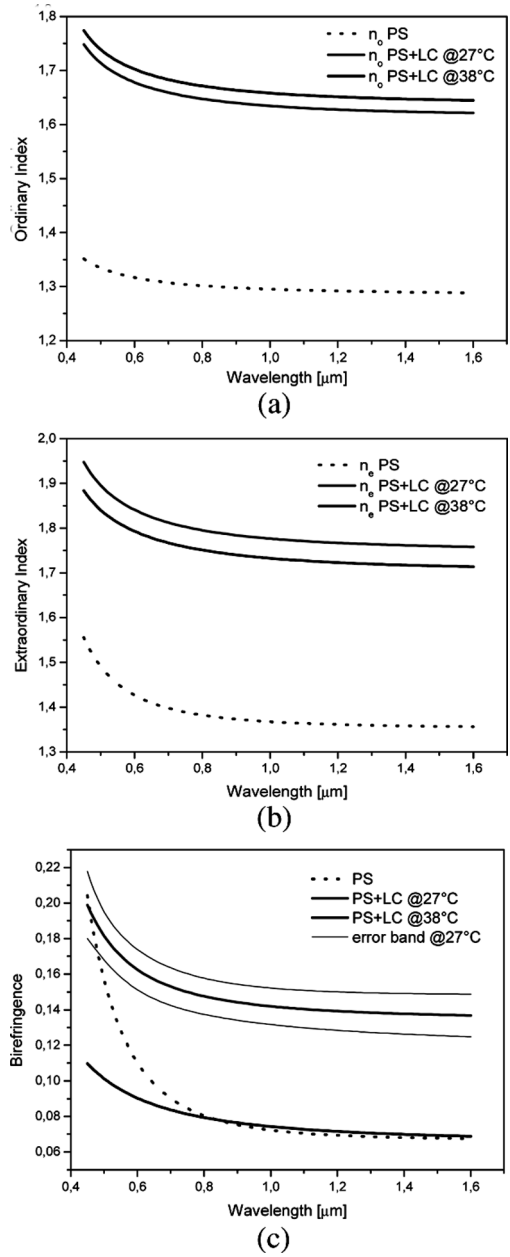

FIGURE 5 Ellipsometric results for the PS sample and the LC + PS one @27.0 and 38.0°C: (a) ordinary index, (b) extraordinary index, and (c) anisotropy.

Figure 5c exhibit two important features, specifically bound to the anisotropy of the infiltrated dielectric:

- above the clearing temperature T_c, the birefringence decreases in the visible and not in IR;
- below T_c, the birefringence clearly increases in the whole spectral range, apart from the short wavelength edge.

The explanation of this behavior may be given considering the following scenario. PS birefringence is due to the form anisotropy exhibited by this material when pores are mostly parallel to each other. The birefringence shown by the whole infiltrated sample is obtained considering not only the depressive effect due to the lowering of the optical contrast between pores and Silicon, but also adding the contribution of the LC birefringence. One should also take into account the relative fractions of the component materials, (PS, LC, and air) and the relative orientation of their optical axes. Thus, from the behavior below T_c, we can suppose that the two optical axis orientations are very close each other, and this is compatible with parallel orientation along the pores of LC director in the nematic phase, as also found in literature [2]. Moreover, from the behavior above T_c, we can suppose that a residual partial anisotropy of the LC material, induced by the strong confinement and quite high surface-to-volume ratio, is still present. Thus, in the NIR range, the residual LC birefringence compensates the expected decrease of the PS birefringence upon infiltration. However, in the visible part of the spectrum, the effect is only to lower the expected birefringence decrease. In fact, the birefringence dispersion curves for PS and for LC exhibit very different shape in the visible, the former being much steeper than the latter one.

CONCLUSIONS AND PERSPECTIVES

We made an optical characterization of liquid crystal infiltrated porous silicon. Ellipsometry can give also interesting information on morphology. LC fills on average about the 52% of the pore volume: 61% at the layer top and less than 31% at the bottom. We expect a higher degree of infiltration by using PS oxidized structure. The found preferred orientation of the LC director is parallel to the pore columns because the layer birefringence increases when the LC is in the nematic phase. A temperature modulation of an infiltrated sample across the LC clearing point can induce a dramatic modulation of its optical properties.

Other models of EMA layer (Landau-Lifshitz/Looyenga, Lorentz-Lorenz etc.) will be used in further simulations to extract the average LC refractive indices from the layer ones.

We believe that inclusion of soft materials with a huge tunability of optical properties, like liquid crystals, can give a new impulse to the silicon based optoelectronics, through the development of a new family of porous silicon based devices.

REFERENCES

[1] Ghulinyan, M., Oton, C. J., Bonetti, G., Gaburro, Z., & Pavesi, L. (2003). *J. Appl. Phys.*, *93*, 9724.
[2] Weiss, S. M., Ouyang, H., Zhang, J., & Fauchet, P. M., (2005). *Optics Express*, *13*, 1090.
[3] Moretti, L., Rea, I., Rotiroti, L., Rendina, I., Abbate, G., Marino, A., & De Stefano, L. (2006). *Optics Express*, Vol. 14, 6264–6272.
[4] Woollam, J. A., Johs, B., Herzinger, C. M., Hilfiker, J. N., Synowicki, R., & Bungay, C. (1999). *Proc. SPIE, CR72, Part I 3–28 and Part II*, 29–58.
[5] Jellison, G. E. (1998). *Thin Solid Films*, *313–314*, 33–39.
[6] Hilfiker, J. N., Herzinger, C. M., Wagner, T., Marino, A., Del Gais, G., & Abbate, G. (2004). *Thin Solid Films*, *455–456*, 591.
[7] Aspnes, D. E. (1979). *Physical Review B*, *20*, 3292–3302.
[8] Zangooie, U., S., Bjorklund, R., & Arwin, H. (1998). *Thin Solid Films*, 313–314.
[9] Künzner, N., Diener, J., Gross, E., Kovalev, D. Timoshenko, Yu, V., & Fujii, M. (2005). *Physical Review B71*, 195304.